Dark Matter Equation of State through Cosmic History

Michael Kopp,[1,2,*] Constantinos Skordis,[1,2,†] Daniel B Thomas,[3,2,‡] and Stéphane Ilić[1,§]

[1]*CEICO, Institute of Physics of the Czech Academy of Sciences, Na Slovance 2, Praha 8, Czech Republic*
[2]*Department of Physics, University of Cyprus, 1, Panepistimiou Street, 2109 Aglantzia, Cyprus*
[3]*Jodrell Bank Centre for Astrophysics, School of Physics and Astronomy, The University of Manchester,
Manchester M13 9PL, United Kingdom*

Cold dark matter is a crucial constituent of the current concordance cosmological model. Having a vanishing equation of state (EOS), its energy density scales with the inverse cosmic volume and is thus uniquely described by a single number, its present abundance. We test the inverse cosmic volume law for dark matter (DM) by allowing its EOS to vary independently in eight redshift bins in the range $z = 10^5$ and $z = 0$. We use the latest measurements of the cosmic microwave background radiation from the *Planck* satellite and supplement them with baryon acoustic oscillation (BAO) data from the 6dF and SDSS-III BOSS surveys and with the Hubble Space Telescope (HST) key project data. We find no evidence for nonzero EOS in any of the eight redshift bins. With *Planck* data alone, the DM abundance is most strongly constrained around matter-radiation equality $\omega_g^{\mathrm{eq}} = 0.1193^{+0.0036}_{-0.0035}$ (95% C.L.), whereas its present-day value is more weakly constrained: $\omega_g^{(0)} = 0.16^{+0.12}_{-0.10}$ (95% C.L.). Adding BAO or HST data does not significantly change the ω_g^{eq} constraint, while $\omega_g^{(0)}$ tightens to $0.160^{+0.069}_{-0.065}$ (95% C.L.) and $0.124^{+0.081}_{-0.067}$ (95% C.L.), respectively. Our results constrain for the first time the level of "coldness" required of the DM across various cosmological epochs and show that the DM abundance is strictly positive at all times.

Introduction.—Cosmological observations indicate that there is insufficient baryonic matter in the Universe for the correct description of physical processes, if gravitational laws are dictated by general relativity. A natural explanation is that most of the matter fields interact negligibly with light, and are thus called dark matter, but can still be seen through their gravitational effect.

Dark matter (DM) is generally thought to be a stable particle (or particles) not part of the standard model; however, it has so far remained elusive [1–7]. Cosmologically, it is usually modeled as cold dark matter (CDM), which is part of the successful ΛCDM model that is consistent with observations of the cosmic microwave background (CMB) (e.g., [8]), cosmic shear surveys (e.g., [9]), measurements of the background expansion such as BAO probes [10], supernovae distance measurements [11], and the observed abundance of light elements [12].

The CDM model is defined by a phase space distribution function satisfying the collisionless Boltzmann equation with an initially vanishing velocity dispersion and curl. This leads to a background CDM density $\bar{\rho}_c(a) \propto a^{-3}$ (a being the scale factor of the Universe) and equation of state (EOS) $w = 0$, while the linearized density and velocity perturbations satisfy the continuity and pressureless Euler equations. Note that we use w to indicate the EOS of DM and not the EOS of dark energy which we assume to be -1 as in ΛCDM. The resulting model arises naturally in the weakly interacting massive particle paradigm: The candidate particles are effectively collisionless, typically have an EOS $w \sim 10^{-24} a^{-2}$ [13,14] and, thus, are well described by CDM. The QCD axion is another CDM candidate [15].

Not all DM candidates fit into the CDM paradigm, for instance, warm DM [14,16,17], ultralight axions [18,19], collisionless massive neutrinos [20,21], self-interacting massive neutrinos [22,23], Chaplygin gas [24], and self-interacting DM [25]. In addition, DM may interact with other species such as neutrinos [26,27], photons [28,29], dark radiation [30–33], and dark energy [34–36].

Rather than taking the CDM description for granted, we consider it timely to examine whether the data themselves support any deviation from the CDM paradigm and, thus, to further determine or constrain DM properties. For our purpose, we use the generalized dark matter (GDM) model, first proposed by W. Hu [37]. The phenomenology of the GDM model has been thoroughly investigated in Ref. [38], where a connection was found with more fundamental theories, including those of a rich self-interacting dark sector. In addition, the recent work on the effective field theory of large-scale structure (EFT of LSS) [39] suggests that, even for an initially pressureless perfect fluid, the nonlinearities that develop on small scales affect the cosmological background and large-scale linear perturbations, creating an effective pressure and viscosity such as those found in GDM.

The GDM model has been used to constrain DM properties with either constant or specific time dependences of the parameters [40–45]. Here, we allow the DM EOS to vary more freely in time than all previous studies.

The model.—We consider a flat Universe with only scalar perturbations; see [38] for more details and notation. The background density $\bar{\rho}_g$ and pressure $\bar{P}_g$ of the DM evolve according to the conservation law

$$\dot{\bar{\rho}}_g = -3H(1+w)\bar{\rho}_g, \qquad \bar{P}_g = w\bar{\rho}_g, q \qquad (1)$$

where $H = (\dot{a}/a)$ is the Hubble parameter and the overdot denotes derivatives with respect to cosmic time t. The parametric function $w(t)$ is freely specifiable with the case $w = 0$ corresponding to a CDM background ($\bar{\rho}_g = \bar{\rho}_c$). The GDM model has two further free functions: the speed of sound c_s^2 and the (shear) viscosity c_{vis}^2. The EOS w is uncorrelated with the two perturbative parameters c_s^2 and c_{vis}^2, as shown in Ref. [44]; thus, in this work, we set these two to zero and denote this class of GDM models by wDM. Consequently, replacing CDM by wDM in the ΛCDM model leads to ΛwDM.

With this choice, the perturbed wDM fluid equations for the density contrast δ_g and velocity perturbation θ_g are given by

$$\frac{\dot{\delta}_g}{1+w} = 3H\left(\frac{w\delta_g}{1+w} + 3aHc_a^2\theta_g\right) - \left(\frac{1}{2}\dot{h} - \frac{1}{a}\vec{\nabla}^2\theta_g\right),$$

$$\dot{\theta}_g = -H\theta_g, \qquad c_a^2 = \frac{\dot{\bar{P}}_g}{\dot{\bar{\rho}}_g} = w - \frac{\dot{w}}{3H(1+w)}. \qquad (2)$$

Here, c_a^2 is the adiabatic speed of sound and h is a metric perturbation in the synchronous gauge [37,38]. The Euler equation $\dot{\theta}_g = -H\theta_g$ is identical to that of CDM, which implies the solution $\theta_g = 0$. An example of wDM is the combination of CDM and Λ interpreted as a single fluid with $w = -(1 + \bar{\rho}_c/\bar{\rho}_\Lambda)^{-1}$. A large degeneracy between Ω_Λ and w is thus expected at late times (see also [46]).

Methodology.—The wDM fluid equations (1) and (2) were implemented in the Boltzmann code CLASS [47] as in Refs. [38,44]. A sufficiently general time dependence of w was achieved by binning its evolution into $N = 8$ scale factor bins, whose edges are $\tilde{a}_i = 10^{\{0,-1,-1.5,-2,-2.5,-3,-3.5,-4\}}$. The bins were smoothly connected using $w(a) = \text{erf}[\sigma_a^{-1}\ln(a/\tilde{a}_{i+1})](w_i - w_{i+1})/2 + (w_i + w_{i+1})/2$ for $a_{i+1} < a < a_i$, with bin centers $a_i = \sqrt{\tilde{a}_i\tilde{a}_{i+1}}$ for $1 \leq i \leq N-2$ while $a_0 = 1$ and $a_{N-1} = 0$. Because of the aforementioned degeneracy of wDM with CDM and Λ, we chose a wider bin in the late Universe.

The σ_a parameter controls the transition width between bins; it was set to $1/20$ so that the transition is small compared to the bin width. We tested that this choice does not affect our conclusions.

We define a dimensionless scaled wDM density

$$\omega_g \equiv a^3\bar{\rho}_g\frac{8\pi G}{3 \times (100 \text{ km/s/Mpc})^2}. \qquad (3)$$

When $w = 0$ through cosmic history, ω_g is a constant equal to the conventional dimensionless CDM density ω_c. In general, however, ω_g varies over time and is fully determined by the $N + 1$ parameters $\omega_g^{(0)}$ and w_i. We use the notation $\omega_g^{(i)} = \omega_g(a_i)$ and similarly for other functions with subscripts, so that the present-day DM abundance is $\omega_g^{(0)} = \omega_g(a_0)$. For functions without a subscript, we instead write $H_i = H(a_i)$ and $w_i = w(a_i)$.

Our parameter constraints were obtained as in Ref. [44], and we present only brief details here. We used the Markov chain Monte Carlo code MONTEPYTHON [48] and established a convergence of the chains using the Gelman-Rubin criterion [49]. Our total parameter set

$$(\omega_b, \omega_g^{(0)}, H_0, n_s, \tau, \ln 10^{10}A_s, w_i) \qquad (4)$$

consists of six ΛCDM parameters and the eight values w_i. We denote the ΛwDM model with eight bins as "var-w" and the previously studied model [44] with $w = $ const as "const-w." We assumed adiabatic initial conditions.

We used the Planck 2015 data release [50] of the CMB anisotropies power spectra, composed of the low-l T/E/B likelihood and the full TT/TE/EE high-l likelihood with the complete "not-lite" set of nuisance parameters [51]. These likelihoods combined are referred to as Planck power spectra (PPS). We also added selectively the HST key project prior on H_0 [52], BAO from the 6dF Galaxy Survey [53] and the Baryon Oscillation Spectroscopic Survey Sloan Digital Sky Survey [10], and the Planck CMB lensing likelihood (respectively referred to as HST, BAO, and lens hereafter).

We set uniform priors on τ and H_0 such that $0.01 < \tau$ and $45 \leq H_0 \leq 90$, respectively. We used the same priors on Planck nuisance parameters and the same neutrino treatment as in Ref. [44]. The helium fraction was set to $Y_{\text{He}} = 0.24667$ [8].

Results.—Our main results are constraints on the time dependence of DM EOS $w(a)$ and abundance $\omega_g(a)$ shown in Figs. 1 and 2. For comparison, we also show the constraints on the const-w model already discussed in Ref. [44]. We list the 95% confidence regions of all parameters in Table I.

In Fig. 1, we observe that ΛCDM lies in the 99% confidence region of the const-w model, which in turn lies in the 99% confidence region of the var-w model, such that the constraints are nested like the models themselves. There is no evidence for significant deviations of the DM EOS from
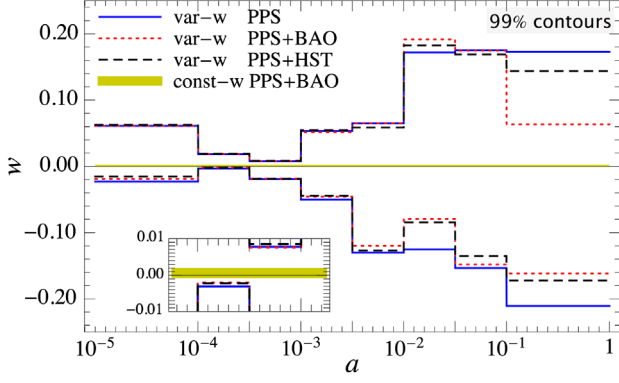
FIG. 1. The 99% confidence regions on the EOS of DM, $w(a)$ for $\sigma_a = 0$. The eight bins are indicated by the large ticks on the a axis. The different line styles correspond to different data sets and models specified in the legend. The inset shows the region between $\tilde{a}_7 = 10^{-4}$ and $\tilde{a}_5 = 10^{-3}$ magnified. Within the const-w narrow stripe lies the ΛCDM model indicated by the black solid line.

0 at any time. Consequently, any model selection criteria will favor ΛCDM.

The constraints on w are the strongest between a_6 and a_5 enclosing the matter-radiation equality $a_{\rm eq} \simeq 3 \times 10^{-4}$ and are about a factor of 2 weaker compared to the const-w model. In other bins, the constraints on w weaken significantly. Adding the BAO or HST data set has only a minor effect on var-w constraints and only tightens limits in the rightmost bin. As was the case for the const-w model [44], adding CMB lensing does not significantly improve the constraints.

Let us now compare in more detail the DM abundance $\omega_g(a)$ of the var-w and const-w models focusing only on the two data set combinations PPS and PPS $+$ BAO $+$ lens. In Fig. 2, we see that, like $w(a)$, ω_g is most tightly constrained between $a_6 = 10^{-3.75}$ and $a_5 = 10^{-3.25}$, in fact almost as
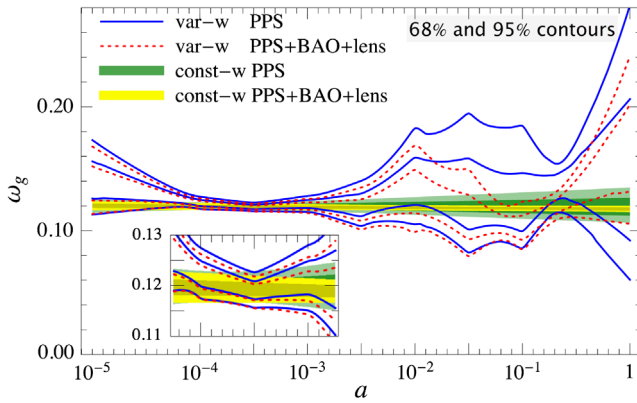

FIG. 2. The 68% and 95% contours of the 1D marginalized posteriors on the DM abundance $\omega_g(a)$. We show the var-w and const-w models, both with two different data sets (PPS and PPS $+$ BAO $+$ lens) as specified in the legend.

tightly as for the const-w model (see the inset in Fig. 2). Around $a = 0.4$, there is a squeeze in the constraints of ω_g from PPS, which extends to $a \sim (0.08, 0.4)$ when BAO or HST are included. At all times, a vanishing DM abundance ($\omega_g = 0$) is inconsistent with the data. More quantitatively, we find for the var-w model at 95% C.L. $\omega_g^{\rm eq} = 0.1193^{+0.0036}_{-0.0035}$ and $\omega_g^{(0)} = 0.16^{+0.12}_{-0.10}$ with PPS only, whereas for PPS $+$ BAO $+$ lens we get $\omega_g^{\rm eq} = 0.1189^{+0.0032}_{-0.0033}$ and $\omega_g^{(0)} = 0.169^{+0.067}_{-0.065}$. For const-$w$-PPS $+$ BAO $+$ lens, we find $\omega_g^{\rm eq} = 0.1193^{+0.0026}_{-0.0026}$, whereas the ΛCDM result is $\omega_c = \omega_g^{\rm eq} = 0.1184^{+0.0022}_{-0.0022}$; see [44].

Consider the tightly constrained region around $a_{\rm eq}$, $a_6 < a < a_5$, as shown in Fig. 2 (see also the inset in the same figure). As discussed in Refs. [37,38], the GDM abundance $\omega_g(a)$ and expansion rate $H(a)$ in the early Universe determine the time of matter-radiation equality and thereby the amount of potential decay until recombination. This in turn sets the relative heights of the first few peaks of the CMB temperature angular power spectrum. Both the const-w and var-w models constrain ω_g around $a_{\rm eq}$ at a similar level (see above). The degeneracy between H_0 and ω_g in the const-w model [44] translates into a degeneracy between H_6 and $\omega_g^{(6)}$ in the var-w model as seen in the left panel in Fig. 3. Indeed, the H_6-$\omega_g^{(6)}$ contours reveal how well the CMB constrains a combination of the expansion rate and the abundance of DM around $a_{\rm eq}$. The

TABLE I. The 95% confidence intervals of var-w parameters.

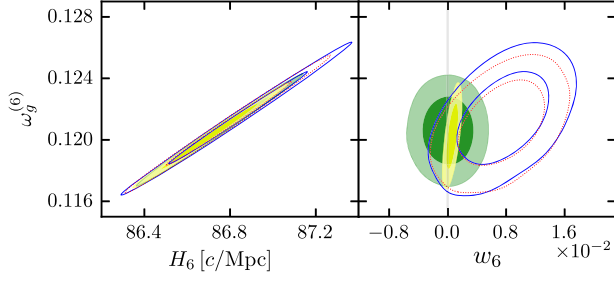|	Data		
Parameter	PPS	PPS $+$ BAO	PPS $+$ HST
$100\omega_b$	$2.221^{+0.041}_{-0.040}$	$2.217^{+0.040}_{-0.038}$	$2.218^{+0.039}_{-0.038}$
$\omega_g^{(0)}$	$0.16^{+0.12}_{-0.10}$	$0.160^{+0.069}_{-0.065}$	$0.124^{+0.081}_{-0.067}$
H_0 [km/s/Mpc]	< 65.9	$66.6^{+3.7}_{-4.0}$	$72.3^{+4.5}_{-4.6}$
n_s	$0.974^{+0.021}_{-0.020}$	$0.974^{+0.020}_{-0.020}$	$0.977^{+0.020}_{-0.020}$
τ	$0.072^{+0.039}_{-0.035}$	$0.076^{+0.040}_{-0.034}$	$0.076^{+0.037}_{-0.034}$
$\ln(10^{10}A_s)$	$3.085^{+0.076}_{-0.069}$	$3.096^{+0.078}_{-0.067}$	$3.096^{+0.073}_{-0.067}$
w_0	$-0.03^{+0.17}_{-0.14}$	$-0.056^{+0.091}_{-0.083}$	$-0.01^{+0.12}_{-0.13}$
w_1	$0.01^{+0.13}_{-0.13}$	$0.02^{+0.12}_{-0.13}$	$0.02^{+0.12}_{-0.12}$
w_2	$0.02^{+0.12}_{-0.11}$	$0.05^{+0.10}_{-0.10}$	$0.05^{+0.11}_{-0.10}$
w_3	$-0.044^{+0.075}_{-0.072}$	$-0.036^{+0.072}_{-0.068}$	$-0.041^{+0.075}_{-0.067}$
w_4	$0.002^{+0.038}_{-0.039}$	$0.005^{+0.036}_{-0.038}$	$0.005^{+0.038}_{-0.038}$
w_5	$-0.006^{+0.011}_{-0.010}$	$-0.006^{+0.010}_{-0.010}$	$-0.005^{+0.011}_{-0.010}$
w_6	$0.0078^{+0.0079}_{-0.0081}$	$0.0084^{+0.0078}_{-0.0079}$	$0.0085^{+0.0080}_{-0.0080}$
w_7	$0.021^{+0.031}_{-0.032}$	$0.022^{+0.030}_{-0.031}$	$0.025^{+0.029}_{-0.030}$
$\Omega_\Lambda^{(0)}$	$0.34^{+0.45}_{-0.58}$	$0.58^{+0.18}_{-0.21}$	$0.72^{+0.14}_{-0.16}$
σ_8	$0.71^{+0.45}_{-0.36}$	$0.72^{+0.27}_{-0.23}$	$0.91^{+0.43}_{-0.39}$

FIG. 3. The 68% and 95% contours of 2D marginalized posteriors of $\omega_g^{(6)}$-H_6 (left) and $\omega_g^{(6)}$-w_6 (right). The line styles and colors are as in Figs. 2 and 4.
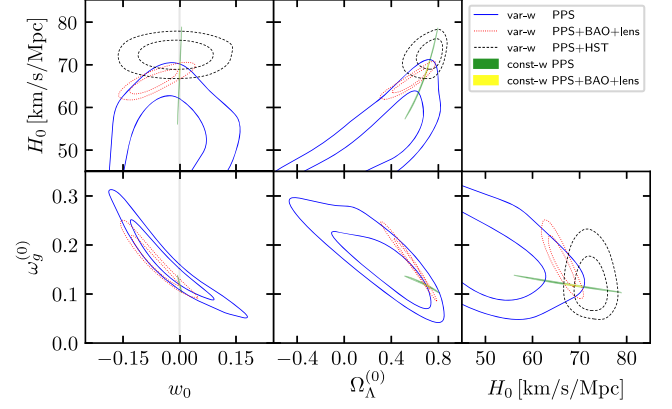

FIG. 4. The 68% and 95% contours of 2D marginalized posteriors for combinations of parameters in the set $\{H_0, w_0, \omega_g^{(0)}, \Omega_\Lambda\}$. The PPS + HST contours in the $\omega_g^{(0)}$-w_0 and $\omega_g^{(0)}$-$\Omega_\Lambda^{(0)}$ panels are not displayed, as they are very similar to PPS + BAO(+lens).

degeneracy between w-ω_g [38,44] in the const-w model due to the same effect is also seen as a degeneracy between w_6 and $\omega_g^{(6)}$ (right panel in Fig. 3); however, in the var-w model, it is weakened, as w_6 has only an indirect effect on $a_{\rm eq}$, contrary to $\omega_g^{(6)}$. Similar correlations exist for H_5-$\omega_g^{(5)}$ and $\omega_g^{(5)}$-w_5 but in the opposite direction.

The origin of the squeeze around $a \sim (0.08\text{--}0.4)$ is of an entirely different nature. The angular diameter distance d_A^* to the last scattering surface is given by

$$d_A^* = a_* \int_{a_*}^{1} d\ln a \,(aH)^{-1} = a_*(\eta_0 - \eta_*). \qquad (5)$$

Here, the second equality has been written in terms of the conformal time ($\eta = \int dt/a$) today, η_0, and at the last scattering surface, η_*. The largest contribution to d_A^* comes from the first $\ln a$ bin where η grows from ~ 4000 to $\sim 14\,000$ Mpc and constitutes $\sim 70\%$ of the total. This contribution can be strongly constrained by geometric probes. Within the first scale factor bin, we have $H = \sqrt{\omega_g^{(0)}(a^{-3(1+w_0)} - 1) + H_0^2}$ (with H and H_0 in units of 100 km/s/Mpc). Hence, for a one-parameter family of $\omega_g^{(0)}$ and w_0, the combination $(aH)^{-1}$ is approximately constant. As this is the largest contributor to d_A^*, we expect w_0 and $\omega_g^{(0)}$ to be anticorrelated, as is indeed observed in Fig. 4 (lower left panel). The inclusion of BAO or HST data significantly improves and shifts the constraints on $\eta(a)$ and is, in turn, reflected in the ω_g and w constraints.

For the var-w model, PPS alone allows for very low H_0, as low as 45 km/s/Mpc, corresponding to our hard prior on H_0; see the blue contours in the top left and bottom right panels in Fig. 4. Adding BAO (red dotted lines) or HST (black dashed lines) shrinks the posteriors and also moves the mean of H_0 back towards the range consistent with the const-w model [44]. BAO (and also HST) data lead to a degeneracy between H_0 and w_0 and between H_0 and $\omega_g^{(0)}$, as in the const-w model. However, as the present-day values of H and ω_g are no longer anchored to their early Universe

values, the degeneracy axis is rotated and the contours are not as flattened.

In the middle panels in Fig. 4, we display the 2D marginalized posteriors of the $H_0 - \Omega_\Lambda$ and $\omega_g^{(0)} - \Omega_\Lambda$ planes. As ω_b is well constrained, wDM and Λ are the only relevant species in the late (flat) Universe and are expected to have their abundances anticorrelated. Indeed, the parameter $\omega_g^{(0)}$ is anticorrelated with $\Omega_\Lambda^{(0)}$ for all data sets. The combination of CDM and Λ may be modeled by wDM; in that model, however, w changes steeply only within the w_0 bin so that this behavior is unaffected. When BAO or HST data are included, the slope and size of the contours change strongly as the late Universe behavior dissociates from the early Universe in the var-w model. The negative values of $\Omega_\Lambda^{(0)}$ are correlated with the low values of H_0, and, while allowed by PPS, they disappear when H_0 is better constrained after including BAO or HST data.

Implications.—In the wDM model, the DM abundance ω_g may deviate from its expected (constant) CDM value throughout cosmic history, causing only minimal changes to the clustering properties of DM. Hence, the constraints on w and ω_g are conservative. One could also conservatively allow for general $c_s^2(a, k)$ and $c_{\rm vis}^2(a, k)$ and marginalize over them. However, as w is almost uncorrelated with c_s^2 and $c_{\rm vis}^2$, we expect such a procedure to give constraints similar to those here. In the cases of warm DM and EFT of LSS, the parameters w, c_s^2, and $c_{\rm vis}^2$ are interrelated so that the w constraints will be driven by c_s^2 and $c_{\rm vis}^2$ and, hence, tightened further [14,45]. Adding a spatial curvature and/or neutrino mass would likely widen the ω_g constraints on the squeeze at $a \sim \{0.08\text{--}0.4\}$ [54] and in the latter case on the tightly constrained region around $a_{\rm eq}$ as well.

When applying our constraints to generic theories of dark matter, including those coming from modifications of gravity, one must keep in mind our underlying assumption of adiabaticity. As models of modified gravity will typically have additional fields leading to more types of isocurvature modes, we expect our constraints to be less applicable in those cases. However, within our adiabatic assumption, we expect our constraints to be valid for any theory of dark matter or modified gravity. The cosmological background in any such theory will have to evolve as in ΛCDM (see, for example, [55]), around matter-radiation equality, and before decoupling. Typical examples include DM-DE coupled models [34–36]. Explicit realizations where a CDM-like background decays into DE are given by the quasidilaton models of massive gravity [56,57] and by axion models [58].

Conclusion.—We have constrained the EOS w and abundance ω_g of dark matter, in eight temporal bins covering five decades in cosmic scale factor, using the CMB data from the *Planck* satellite, and separately including BAO and HST data. We found that w is consistent with zero and the DM abundance is strictly positive at all cosmological epochs considered here (see Figs. 1 and 2), and thus the concordance ΛCDM model remains unchallenged. This is the first time that the level of DM "coldness" across cosmic time has been explicitly constrained.

*kopp@fzu.cz
†skordis@fzu.cz
‡daniel.thomas-2@manchester.ac.uk
§ilic@fzu.cz

[1] R. Agnese *et al.*, Phys. Rev. Lett. **116**, 071301 (2016).
[2] A. Tan *et al.*, Phys. Rev. Lett. **117**, 121303 (2016).
[3] E. Aprile *et al.*, Phys. Rev. D **94**, 092001 (2016).
[4] J. V. Sloan *et al.*, Phys. Dark Universe **14**, 95 (2016).
[5] D. S. Akerib *et al.*, Phys. Rev. Lett. **118**, 021303 (2017).
[6] F. Petricca *et al.* (CRESST Collaboration), arXiv:1711.07692.
[7] B. M. Brubaker *et al.*, Phys. Rev. Lett. **118**, 061302 (2017).
[8] P. A. R. Ade *et al.* (Planck Collaboration), Astron. Astrophys. **594**, A13 (2016).
[9] T. M. C. Abbott *et al.*, arXiv:1801.03181.
[10] L. Anderson *et al.*, Mon. Not. R. Astron. Soc. **441**, 24 (2014).
[11] D. O. Jones *et al.*, Astrophys. J. **857**, 51 (2018).
[12] M. Peimbert, V. Luridiana, and A. Peimbert, Astrophys. J. **666**, 636 (2007).
[13] A. M. Green, S. Hofmann, and D. J. Schwarz, J. Cosmol. Astropart. Phys. 08 (2005) 003.
[14] C. Armendariz-Picon and J. T. Neelakanta, J. Cosmol. Astropart. Phys. 03 (2014) 049.
[15] L. Visinelli and P. Gondolo, Phys. Rev. Lett. **113**, 011802 (2014).
[16] S. Dodelson and L. M. Widrow, Phys. Rev. Lett. **72**, 17 (1994).
[17] O. F. Piattella, L. Casarini, J. C. Fabris, and J. A. de Freitas Pacheco, J. Cosmol. Astropart. Phys. 02 (2016) 024.
[18] W. Hu, R. Barkana, and A. Gruzinov, Phys. Rev. Lett. **85**, 1158 (2000).
[19] R. Hlozek, D. Grin, D. J. E. Marsh, and P. G. Ferreira, Phys. Rev. D **91**, 103512 (2015).
[20] M. Shoji and E. Komatsu, Phys. Rev. D **82**, 089901(E) (2010).
[21] J. Lesgourgues and T. Tram, J. Cosmol. Astropart. Phys. 09 (2011) 032.
[22] F.-Y. Cyr-Racine and K. Sigurdson, Phys. Rev. D **90**, 123533 (2014).
[23] I. M. Oldengott, C. Rampf, and Y. Y. Y. Wong, J. Cosmol. Astropart. Phys. 04 (2015) 016.
[24] H. B. Sandvik, M. Tegmark, M. Zaldarriaga, and I. Waga, Phys. Rev. D **69**, 123524 (2004).
[25] D. N. Spergel and P. J. Steinhardt, Phys. Rev. Lett. **84**, 3760 (2000).
[26] P. Serra, F. Zalamea, A. Cooray, G. Mangano, and A. Melchiorri, Phys. Rev. D **81**, 043507 (2010).
[27] R. J. Wilkinson, C. Boehm, and J. Lesgourgues, J. Cosmol. Astropart. Phys. 05 (2014) 011.
[28] C. Boehm, A. Riazuelo, S. H. Hansen, and R. Schaeffer, Phys. Rev. D **66**, 083505 (2002).
[29] R. J. Wilkinson, J. Lesgourgues, and C. Boehm, J. Cosmol. Astropart. Phys. 04 (2014) 026.
[30] F.-Y. Cyr-Racine and K. Sigurdson, Phys. Rev. D **87**, 103515 (2013).
[31] R. Diamanti, E. Giusarma, O. Mena, M. Archidiacono, and A. Melchiorri, Phys. Rev. D **87**, 063509 (2013).
[32] M. A. Buen-Abad, G. Marques-Tavares, and M. Schmaltz, Phys. Rev. D **92**, 023531 (2015).
[33] J. Lesgourgues, G. Marques-Tavares, and M. Schmaltz, J. Cosmol. Astropart. Phys. 02 (2016) 037.
[34] L. Amendola, Mon. Not. R. Astron. Soc. **312**, 521 (2000).
[35] A. Pourtsidou, C. Skordis, and E. J. Copeland, Phys. Rev. D **88**, 083505 (2013).
[36] G. D'Amico, T. Hamill, and N. Kaloper, Phys. Rev. D **94**, 103526 (2016).
[37] W. Hu, Astrophys. J. **506**, 485 (1998).
[38] M. Kopp, C. Skordis, and D. B. Thomas, Phys. Rev. D **94**, 043512 (2016).
[39] D. Baumann, A. Nicolis, L. Senatore, and M. Zaldarriaga, J. Cosmol. Astropart. Phys. 07 (2012) 051.
[40] C. M. Müller, Phys. Rev. D **71**, 047302 (2005).
[41] E. Calabrese, M. Migliaccio, L. Pagano, G. DeTroia, A. Melchiorri, and P. Natoli, Phys. Rev. D **80**, 063539 (2009).
[42] S. Kumar and L. Xu, Phys. Lett. B **737**, 244 (2014).
[43] L. Xu and Y. Chang, Phys. Rev. D **88**, 127301 (2013).
[44] D. B. Thomas, M. Kopp, and C. Skordis, Astrophys. J. **830**, 155 (2016).
[45] M. Kunz, S. Nesseris, and I. Sawicki, Phys. Rev. D **94**, 023510 (2016).

[46] I. Tutusaus, B. Lamine, A. Blanchard, A. Dupays, Y. Rousset, and Y. Zolnierowski, Phys. Rev. D **94**, 123515 (2016).

[47] D. Blas, J. Lesgourgues, and T. Tram, J. Cosmol. Astropart. Phys. 07 (2011) 034.

[48] B. Audren, J. Lesgourgues, K. Benabed, and S. Prunet, J. Cosmol. Astropart. Phys. 02 (2013) 001.

[49] D. B. R. Andrew Gelman, Stat. Sci. **7**, 457 (1992).

[50] N. Aghanim *et al.* (Planck Collaboration), Astron. Astrophys. **594**, A11 (2016).

[51] For full details, see the Planck papers and wiki http://wiki .cosmos.esa.int/planckpla2015/index.php/.

[52] A. G. Riess, L. Macri, S. Casertano, H. Lampeitl, H. C. Ferguson, A. V. Filippenko, S. W. Jha, W. Li, and R. Chornock, Astrophys. J. **730**, 119 (2011).

[53] F. Beutler, C. Blake, M. Colless, D. H. Jones, L. Staveley-Smith, L. Campbell, Q. Parker, W. Saunders, and F. Watson, Mon. Not. R. Astron. Soc. **416**, 3017 (2011).

[54] P. G. Ferreira, C. Skordis, and C. Zunckel, Phys. Rev. D **78**, 044043 (2008).

[55] M. Banados, P. G. Ferreira, and C. Skordis, Phys. Rev. D **79**, 063511 (2009).

[56] R. Gannouji, Md. Wali Hossain, M. Sami, and E. N. Saridakis, Phys. Rev. D **87**, 123536 (2013).

[57] S. Anselmi, D. López Nacir, and G. D. Starkman, Phys. Rev. D **92**, 084033 (2015).

[58] T. Kobayashi and P. G. Ferreira, arXiv:1801.09658.